Pattern-Dislocation-Type Dynamical Instability in 1D Optical Feedback Kerr Media with Gaussian Transverse Pumping

E. Louvergneaux

Laboratoire de Physique des Lasers, Atomes et Molécules, UMR 8523, Centre d'Etudes et de Recherches Lasers et Applications, Université des Sciences et Technologies de Lille, F-59655 Villeneuve d'Ascq Cedex, France

(Received 25 July 2001; revised manuscript received 5 October 2001; published 26 November 2001)

We study experimentally and numerically the secondary instability corresponding to the destabilization of stationary transverse roll patterns appearing in a 1D liquid crystal layer subjected to optical feedback. This dynamical instability appears as roll dislocations in the spatiotemporal diagrams. We show that it originates from the *Gaussian* spatial transverse dependence of a control parameter and that its corresponding mechanism is the selection of a local unstable wave number. This instability is the optical counterpart of the *ramp-induced Eckhaus instability* observed in hydrodynamics.

DOI: 10.1103/PhysRevLett.87.244501 PACS numbers: 47.54.+r, 05.45.–a, 42.65.Sf, 61.30.Gd

Many dissipative systems, when driven far from equilibrium, can undergo a primary instability from a spatially uniform state to a state with spatial periodicity when a threshold value of an external forcing parameter, let us say, R is exceeded. Examples are Rayleigh-Benard convection [1], Taylor vortex flow [2], electroconvection in liquid crystals [3], chemical reactions [4], optical feedback systems [5], etc. The question then arises as to how the emerged patterns destabilize as R is further increased. The study of these secondary instabilities has been generally carried out for "ideal infinite uniform systems" with periodic boundary conditions for the theoretical case and large aspect ratios for the experimental one. This leads to the well-known Eckhaus, zigzag, ... instabilities [6]. However, many real systems cannot be considered as uniform since their control parameters present spatial variations. The consequences of these spatial dependences have been shown to induce a particular type of secondary instability in hydrodynamics, the *ramp-induced Eckhaus instability* [7–9] which has been also evidenced in optics in the stationary patterns appearing inside the spectrum of a fiber laser [10]. In the domain of optical transverse patterns, the smooth spatial variations are unavoidable because of the Gaussian profile of laser beams or else curved mirrors and should lead to the same kind of instability as suggested in Ref. [10].

In this Letter, we show that taking into account explicitly these spatial dependences of control parameters in optical transverse patterns leads to a spatial secondary instability which appears to be generic to systems with "bell shaped" variation of the parameters. It constitutes the counterpart of the ramp-induced Eckhaus instability in hydrodynamics. More precisely, we show that the Gaussian transverse spatial dependence of the laser beam control parameter induces a dislocation-type secondary instability. This occurs through recurrent annihilation or creation of cells (depending on the sign of the nonlinearity) appearing as dislocations in the spatiotemporal diagrams of output 1D transverse pattern. We also show that the Gaussian profile of the pump intensity leads to a selection mechanism of a local unstable wave number as in Refs. [8–10].

A simple optical system which gives rise to spontaneous transverse pattern formation is a thin slice of Kerr medium irradiated by a Gaussian laser beam and a single feedback mirror at a distance d from the Kerr slice, which reflects the transmitted light backwards into the medium [11], as shown in Fig. 1. Pattern formation in such a system usually occurs through hexagon and roll formation at threshold [5,12,13]. The Kerr-like medium is a 50 μm thick cell of homeotropically aligned E_7 nematic liquid crystal (LC). The cell is tilted with an angle of 45° with respect to the optical axis in order to maximize the nonlinear effective Kerr coefficient n_2 [13]. Two identical lenses set in a "4f-type" arrangement lead to a virtual mirror M', shifted by a distance $4f$ with respect to M. Note that this allows for positive and negative equivalent feedback paths d. It was shown that changing the sign of d was equivalent in changing the sign of the Kerr nonlinearity [14]. Thus, it is negative for a negative optical distance d yielding a defocusing-type system. The pump beam is emitted by a linearly polarized frequency-doubled $NdYVO_4$ laser at 532 nm. The laser beam diameter can be continuously and independently varied in the two transverse directions by means of two cylindrical lens telescopes. Let us introduce the aspect ratio η which reads

$$\eta = \frac{2w}{\Lambda_\infty}, \tag{1}$$

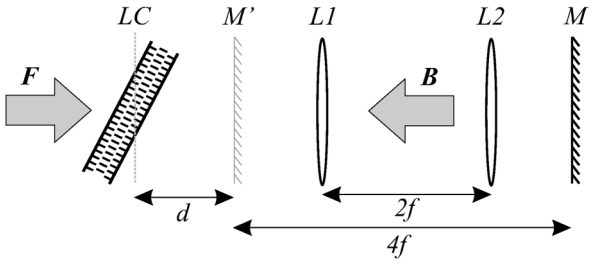

FIG. 1. Scheme of the experimental setup; LC: liquid crystal layer; L_1, L_2: lenses of focal length f; M (respectively, M'): real (respectively, virtual) feedback mirror; F, B: forward and backward optical fields.

where $2w$ is the input beam diameter at LC plane and Λ_∞ is the critical wavelength of pattern obtained for a plane wave input beam at threshold. In our experiment, a one-dimensional (1D) transverse laser beam corresponds to η close to unity in one direction and much larger than unity (typically 20–40) in the orthogonal one. This allows one to obtain 1D patterns composed of one line of cells as shown in Fig. 2(h). The reflected beam is collected on charge-coupled device cameras through near or far field imaging. Two control parameters are accessible to explore the patterns and their dynamics, namely, the feedback length d and the laser intensity I.

Spontaneous 1D pattern formation is observed [Fig. 2(h)] as the laser intensity exceeds some threshold value I_{th}. The transverse modulation of the intensity corresponds to the destabilization of the critical wave number q_{th} appearing at the primary instability threshold. The evolution of the pattern is illustrated using the standard spatiotemporal plot for 1D systems with space and time as horizontal axis and vertical axis, respectively. Figure 2(a)–2(c) shows the way through which the patterns appear and destabilize in the presence of a Gaussian input field [Fig. 2(g)] in different feedback situations. Figure 2(a) shows the reference pattern which appears just above threshold I_{th}. It corresponds to a stationary wave extending over the central part of the transverse profile with an approximately constant wave number q_{th} (the variation of q_{th} over the transverse profile is typically less than 2% when I is 1% above threshold). This pattern remains stationary up to an intensity value I_2 where it is destabilized by recurrent creation (respectively, annihilation) of cells for negative (respectively, positive) values of the optical feedback path d as illustrated in Fig. 2(b) [respectively, Fig. 2(c)]. We have observed that cell creation and annihilation are always accompanied by outward (respectively, inward) drift of the remaining cell pattern and always appear in the central part of the pattern. For larger beam diameter (typically $\eta > 40$), the dislocations are distributed more randomly in a wider central region of the spatiotemporal diagrams. Although the general scheme of pattern evolution is similar for both signs of d, the specific values of thresholds and occurrence of dislocations are quite different for positive and negative values of d. For instance, for a value of η approximately equal to 36, the ratio between the second and the first threshold I_2/I_{th} is, e.g., 2.3 (respectively, 1.7) with positive (respectively, negative) d. Moreover, the occurrence of successive dislocations close to I_2 is almost regular for negative d (time fluctuations in recurrence periods are less than 10%), while no regularity is observed for positive d.

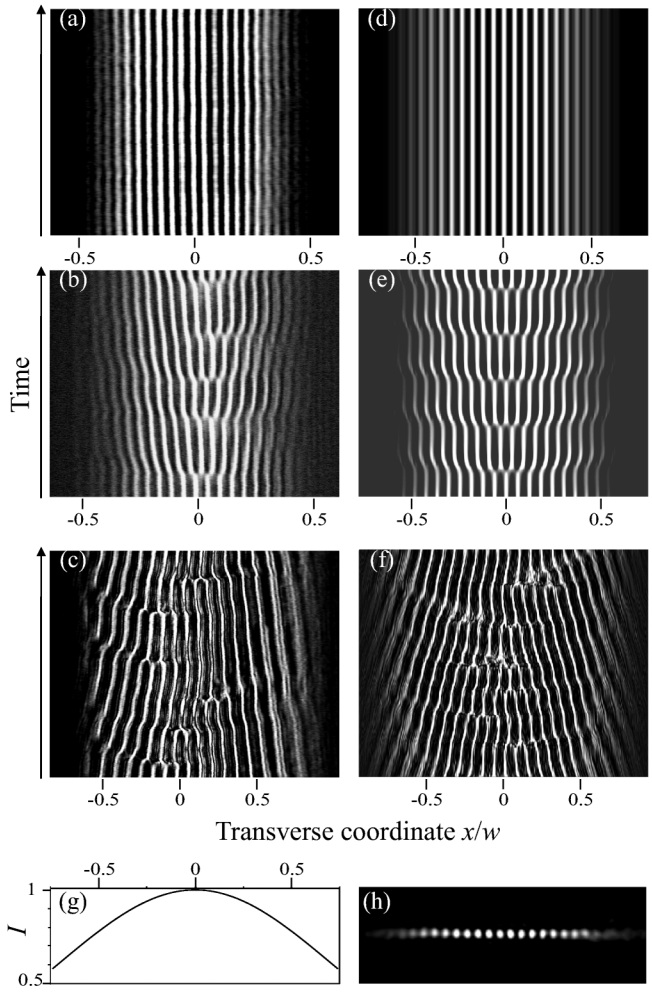

FIG. 2. (a)–(c) Spatiotemporal diagrams of experimental pattern dynamics, (a) stationary; (b),(c) unstable. (d)–(f) Corresponding numerical simulations. (g) Transverse intensity profile. (h) Typical 1D transverse pattern. (a),(b),(d),(e) [respectively, (c),(f)] Positive (respectively, negative) feedback length d. Recording times are 512 s for experiments and 100τ for numerical simulations. From (a) to (f): $\eta = 36; 36; 20; 36; 36; 21$ and $I/I_{\text{th}} = 1.3; 1.6; 3; 1.14; 1.28; 3.6$.

The theoretical study of pattern destabilization can be performed in the framework of the model commonly used to describe the spatiotemporal dynamics of liquid crystal under the presence of an external feedback. The Kerr equation for refractive index n which captures most of the relevant dynamics of the liquid crystal reads [15]

$$-l_D^2 \frac{\partial^2 n}{\partial x^2} + \tau \frac{\partial n}{\partial t} + n = |F|^2 + |B|^2. \qquad (2)$$

The Kerr effect, assumed to be due to photoexcitation, relaxes to zero with a time constant τ. The diffusion length l_D inside the crystal is much larger than the optical wavelength λ_0 thus removing the transverse interference effects. The small thickness of the Kerr medium allows neglecting light diffraction along the sample [11]. F and B are the forward field and the backward field, respectively. Equation (2) must be completed by the two following equations that govern light propagation through the sample and over the feedback loop, respectively:

$$\frac{\partial F}{\partial z} = i\chi n F, \quad \text{and} \quad \frac{\partial F}{\partial z} = \frac{-i}{2k_0} \nabla_\perp^2 F\,. \qquad (3)$$

χ parametrizes the Kerr effect (positive for a focusing medium, $d > 0$) and k_0 is the laser field wave number. The profile of the forward propagation field is assumed to be Gaussian so that $F = F_0 e^{-(x^2/w^2)}$, with w the beam radius at the sample.

The numerical code developed for solving Eqs. (2) and (3) uses a Fourier-transform routine to propagate the fields in free space and a Runge-Kutta method of order 8 to integrate the equation of refractive index. As shown in Fig. 2(d), a pattern appears at threshold $F_{0\text{th}}$ which remains stationary until it is destabilized for a higher F_0 value either by cell creations [Fig. 2(e)] or annihilations [Fig. 2(f)] in agreement with experimental observations for, respectively, negative or positive feedback d values. The properties of regularity in successive dislocation occurrence also correspond to those described in the experimental pattern recordings. Thus, the dynamical behaviors obtained from numerical simulations are in good qualitative agreement with those experimentally observed.

Let us discuss now the mechanism through which this instability arises. It is clearly linked to cell drift since cell creation implies that the already present cells move away (i.e., the wave number in that place locally decreases). To go further into the discussion, we need a local characterization of the pattern. It can be obtained by considering the Hilbert transform of the backward intensity which provides us with a measure of the local wave number $q(x)$ [16]. Figure 3 shows the transverse profiles of $q(x)$ for increasing intensities for numerical simulations and experiments in the stationary regimes [e.g., Figs. 2(d) and 2(a)]. It is obvious that the local wave number $q(x)$ is completely determined by the variation of the intensity profile [Fig. 2(g)] with a minimum value at the center, i.e., at the maximum of the pump profile for $d < 0$. The important point here is that the gradient of $q(x)$ increases with light intensity as shown by the arrows in Fig. 3. Following this scheme, the intensity threshold for the secondary instability is reached when the local wave number $q(x)$ reaches an unstable domain, e.g., $q(0) < 101w^{-1}$ in the conditions of Fig. 3(a). Beyond this value a cell creation always appears at $q(0)$. This fixes the maximum variation of q beyond which q is smaller than the smallest stable q; the local spacing between two neighbor cells then becomes too large thus leading to the creation of a new cell. Similar experiments and simulations in the positive d case exhibit the opposite dependence on the intensity.

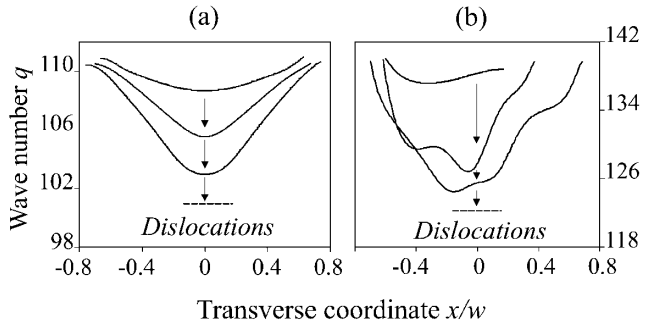

FIG. 3. Evolution of the transverse profiles of the wave number q (measured in units of w^{-1}) for various intensities. (a) Numerical simulations; (b) experiments. $I/I_{\text{th}} = (a)$ 1.01; 1.14; 1.25, (b) 1.37; 1.54; 1.6. $\eta = 36$. The arrows show the way of $q(x)$ variation with intensity. The dashed line symbolizes very locally the secondary instability threshold. The ripples seen on (b) are caused by inhomogeneities in the sample.

Thus, the Hilbert transform shows that the dislocation mechanism corresponds to the selection of an unstable wave number. This selection is local and results from the transverse profile of q which is induced by the transverse dependence of the intensity. An important feature here is that the instability arises in the region of the maximum intensity, i.e., where the transverse dependence is *parabolic*. The wing parts of the Gaussian profile play no role in the dynamics since they are well below threshold. The relevance of the parabolic part in the dynamics of transverse pattern formation has already been evidenced in systems under inhomogeneous pumping [17]. Thus, the origin of the dislocation instability is directly related to the parabolic transverse dependence of the control parameter $I(x)$ [Fig. 2(g)].

The instability described in this Letter is induced by the Gaussian spatial properties of a control parameter (R) and does not correspond to the standard secondary instabilities such as, e.g., Eckhaus or zigzag instabilities. Secondary instabilities induced by spatial dependence of a control parameter have been evidenced in hydrodynamics by Riecke and Paap [8] in a ramped Taylor vortex flow (TVF) and more recently in optics in the emitted optical power spectrum of a fiber laser [10]. Both of these experiments showed that the spatial dependence of R selects a wave number q outside the Eckhaus stable wave number band. A dislocation then appears each time this wave number crosses the band limit given by the linear stability analysis of the uniform system. Another feature is that the wave number selection from its threshold value to its unstable value is completely determined by the spatial gradient of the considered control parameter (the angle of the ramp in the TVF, η in optics). This leads to different paths in the (I, q) stability diagram and different values of $q(I_2)$. We can follow experimentally the progressive selection of q and consider that the appearance of dislocations can be used to locate the Eckhaus band for a given η. Figure 4 displays the evolution of q versus the input intensity for different values of the aspect ratio η in the experimental defocusing case. The evolutions of q show a nonmonotonic behavior for $\eta > 30$. Above this value, q decreases until it reaches a value $q(I_2)$ where a dislocation appears in the pattern (denoted D in Fig. 4). This shows that the selected wave number depends on both the intensity I and the aspect ratio η. The same behavior is observed for the positive case except that q always increases from the first to the second instability thresholds. An advantage can be taken from this to select any required wave

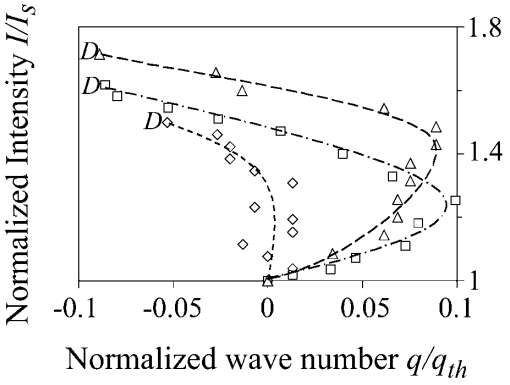

FIG. 4. Experimental evolution of q with intensity in the (I, q) diagram for different aspect ratios. $\eta = 30$ (diamonds), 36 (triangles), and 49 (squares). D denotes the boundary of the secondary instability region.

number in the stable state band by a suitable choice of the aspect ratio η.

In conclusion, we have evidenced a secondary instability present in 1D systems with bell shaped transverse spatial dependence of one control parameter, such as the Gaussian profile of the intensity in optics. It appears as dislocations in the spatiotemporal diagrams of pattern evolution. It reminds us of dislocations in the stationary transverse patterns observed in, e.g., liquid crystal electroconvection but is completely different since it finds its origin in the transverse spatial dependence of a control parameter as opposite to electroconvection where the parameters are spatially uniform. The basic mechanism and wave number selection can be related to that observed in hydrodynamics. Here, the Gaussian profile can be seen as two connected identical ramps, each of them inducing a drift [18]. The smooth connection locks the drifts until the q gradient from boundary to bulk can no longer be "absorbed" by the system then leading to the creation/annihilation of a cell. Finally, it suggests that any 1D pattern forming system involving a control parameter with "parabolic" dependence such as the central part of Gaussian shapes can undergo this kind of instability. The open question then arises to the role of this parabolic spatial dependence in 2D secondary instabilities since, e.g., the stabilization mechanism has been observed in a 2D drift instability [19].

E. L. acknowledges the group of N. Isaert for its assistance in the realization of liquid crystal samples, C. Szwaj and S. Bielawski for helpful discussions in the understanding of the instability mechanism, and especially P. Glorieux for his support in the achievement of this project and his help in the writing of this Letter. The Centre d'Etudes et de Recherches Lasers et Applications (CERLA) is supported by the Ministère chargé de la Recherche, the Région Nord/Pas de Calais, and the Fonds Européen de Développement Economique des Régions.

[1] A. Schlüter, D. Lortz, and F. Busse, J. Fluid Mech. **23**, 129 (1965).
[2] R. C. DiPrima and H. L. Swinney, in *Hydrodynamic Instabilities and Transition to Turbulence,* edited by H. L. Swinney and J. P. Gollub (Springer, Berlin, 1981).
[3] L. Kramer and W. Pesch, in *Pattern Formation in Liquid Crystals,* edited by A. Buka and L. Kramer (Springer, New York, 1996).
[4] D. Feinn, P. Ortuleva, W. Scalf, S. Schmidt, and M. Wolff, J. Chem. Phys. **69**, 27 (1978).
[5] T. Ackemann and W. Lange, Appl. Phys. B **72**, 21 (2000).
[6] M. C. Cross and P. C. Hohenberg, Rev. Mod. Phys. **65**, 851 (1993).
[7] Y. Pomeau and P. Manneville, J. Phys. (Paris), Lett. **40**, L609 (1979); L. Kramer, E. Ben-Jacob, H. Brand, and M. C. Cross, Phys. Rev. Lett. **49**, 1891 (1982).
[8] H. Riecke and H. G. Paap, Phys. Rev. Lett. **59**, 2570 (1987).
[9] M. A. Dominguez-Lerma, D. S. Cannell, and G. Ahlers, Phys. Rev. A **34**, 4956 (1986).
[10] J. Plumecoq, C. Szwaj, D. Derozier, M. Lefranc, and S. Bielawski, Phys. Rev. A **64**, 061801(R) (2001).
[11] W. J. Firth, J. Mod. Opt. **37**, 151 (1990).
[12] G. D'Alessandro and W. J. Firth, Phys. Rev. A **46**, 537 (1992); R. MacDonald and H. Danlewski, Opt. Lett. **20**, 441 (1995); T. Honda, H. Matsumoto, M. Sedlatschek, C. Denz, and T. Tschudi, Opt. Commun. **133**, 293 (1997).
[13] E. Santamato, E. Ciaramella, and M. Tamburrini, Mol. Cryst. Liq. Cryst. **251**, 127 (1994).
[14] E. Ciaramella, M. Tamburrini, and E. Santamato, Appl. Phys. Lett. **63**, 1604 (1993).
[15] R. MacDonald and H. J. Eichler, Opt. Commun. **89**, 289 (1992).
[16] See Sec. 2.2 in P. Bot and I. Mutabazi, Eur. Phys. J. B **13**, 141 (2000).
[17] M. N. Ouarzazi, P. A. Bois, and M. Taki, Phys. Rev. A **53**, 4408 (1996).
[18] I. Rehberg, E. Bodenschatz, B. Winkler, and F. H. Busse, Phys. Rev. Lett. **59**, 282 (1987).
[19] T. Ackemann, B. Schäpers, J. P. Seipenbusch, Yu. A. Logvin, and W. Lange, Chaos Solitons Fractals **10**, 665 (1999).